Food Hydrocolloids 136 (2023) 108289

Contents lists available at ScienceDirect

Food Hydrocolloids

journal homepage: www.elsevier.com/locate/foodhyd

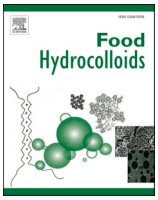

Changes in structure and emulsifying properties of coconut globulin after the atmospheric pressure cold plasma treatment

Yang Chen [a], Mengying Yao [b], Tianyi Yang [a], Yajing Fang [a], Dong Xiang [a], Weimin Zhang [a,c,*]

[a] School of Food Science and Engineering, Hainan University, Hainan, 570228, China
[b] Public Inspection and Testing Center of Gong'an County, Jingzhou, 434300, China
[c] Key Laboratory of Tropical Fruits and Vegetables Quality and Safety for State Market Regulation, Hainan Institute for Food Control, Haikou, 570228, China

ARTICLE INFO

Keywords:
Coconut globulin
Atmospheric pressure cold plasma
Secondary structure
Emulsifying property

ABSTRACT

Atmospheric pressure cold plasma (ACP) treatment, a non-thermal sterilization technology with great potential in coconut milk, can maximize the retention of the taste and flavour. However, it is unavoidable to have an impact on the coconut milk components. In this study, coconut globulin (CG), a component important for coconut milk stability, was selected to explore the effect of the ACP treatment on the structure and emulsifying properties of CG. After the ACP treatment, the structure of CG unfolded, which was the increase in random coils and reduction in intrinsic fluorescence intensity. In addition, the carbonyl and S–S bond content increased, while the free –SH content decreased. Compared with untreated CG (440.57 nm), the particle size of CG after the ACP treatment decreased, especially at 60 kV 60 s (207.63 nm) and 60 kV 90 s (204.20 nm). Simultaneously, poor modification and excessive modification of CG have similar surface hydrophobicity and interfacial tension to untreated CG. Notably, moderate modification (60 kV 60 s and 60 kV 90 s) resulted in the unfolding of CG molecules and the exposure of hydrophobic groups, increasing their adsorption at the oil-water interface. As expected, the emulsifying ability and emulsifying stability of CG were significantly improved after the ACP treatment at 60 kV 60 s and 60 kV 90 s. In conclusion, moderate ACP treatment could improve the emulsifying properties of CG by modifying its structure. This study provides new insights into the effect of ACP on food components during liquid food sterilization.

1. Introduction

Coconut (*Cocos nucifera* L.) belongs to the *Palmae* family, and its products include coconut oil, coconut water, coconut milk, and coconut flour (Kotecka-Majchrzak, Sumara, Fornal, & Montowska, 2020; Ramesh, Krishnan, Praveen, & Hebbar, 2021; Rodsamran & Sothornvit, 2018). Based on its unique characteristics, coconut-related products are very popular. Coconut milk, usually extracted from the coconut meat after pressing or squeezing with or without water, is used as a major ingredient for several cuisines such as curries, bakeries, and desserts (Lu et al., 2019). In coconut milk emulsion, coconut protein acts as a natural emulsifier and adheres to the surface of coconut oil to form an oil in water (O/W) emulsion (Ariyaprakai, Limpachoti, & Pradipasena, 2013; Paixao, Brandao, Araujo, & Korn, 2019). Coconut globulin (CG), the main protein in coconut (accounting for 60–75%), has good emulsifying properties and plays a major role in the stability of coconut milk (Patil & Benjakul, 2017; Surojanametakul et al., 2011; Tangsuphoom & Coupland, 2009).

Coconut milk is rich in protein and oil, which is prone to microbial contamination and needs to be sterilized during processing (Chalupa-Krebzdak, Long, & Bohrer, 2018). The traditional sterilization method of coconut milk is heat sterilization, such as pasteurization and high-temperature instantaneous sterilization (Jermwongruttanachai, Pathaveerat, & Noypitak, 2021). In thermal processing, the change in food structure and loss of texture is common (Tiravibulsin, Lorjaroenphon, Udompijitkul, & Kamonpatana, 2021). In addition, the thermal sterilization process can cause a lot of protein degradation, which affects the emulsion system of coconut milk, including droplet aggregation and delamination (Kunchitwaranont, Chiewchan, & Devahastin, 2019).

As a novel non-thermal sterilization technology, atmospheric pressure cold plasma (ACP) treatment is generated by electrons accelerating in the electric field and colliding with other particles in the air, resulting in the production of charged particles, free radicals, excited atoms, and

* Corresponding author. No. 58 Renmin Road, College of Food Science and Engineering, Hainan University, Haikou, 570228, China..
E-mail address: zhwm1979@163.com (W. Zhang).

https://doi.org/10.1016/j.foodhyd.2022.108289
Received 12 September 2022; Received in revised form 16 October 2022; Accepted 2 November 2022
Available online 8 November 2022

other active species (Liao et al., 2020). The highly active species generated by ACP treatment can damage the cell structures and metabolic activities of microorganisms, which contributes to effectively inactivating microorganisms (Hati, Patel, & Yadav, 2018). Currently, ACP treatment shows great potential in sterilising liquid food, such as fruit juice and milk (Coutinho et al., 2018). In ACP-treated liquid food, the free radicals are mainly ·OH, ·OOH, $O_2\cdot^-$, and ·NO, which can inactivate microorganisms without causing safety problems (Yepez, Illera, Baykara, & Keener, 2022).

The advantages of ACP treatment are operation at low temperatures, short processing times, and efficient sterilization effect with minimal impact on food quality (Kaavya et al., 2022). However, during ACP treatment, a wide range of active species also affect the food ingredients, such as proteins, lipids and polysaccharides (Waghmare, 2021). These changes have an impact on the stability, structure, texture, and sensory properties, thereby affecting the quality of food. However, the biggest challenge of ACP application in food is how to precisely define the operating conditions to achieve effective inactivation of microorganisms while minimizing the impact on food quality. Therefore, it is urgent to study the changes in food ingredients and structure after ACP treatment under different conditions to promote the large-scale application of ACP in food.

This study aims to investigate modifying CG molecules by ACP treatment to improve the emulsifying properties. In this study, ACP-treated CG with different conditions was used to prepare the O/W emulsion. The structure, oxidation degree, aggregation, and interfacial properties of CG were systematically evaluated, and emulsifying properties of CG were characterized. This study is expected to provide a theoretical basis and practical guidance for minimizing the addition of other exogenous emulsifiers and using the ACP treatment to maintain the quality and stability of coconut milk.

2. Materials and methods

2.1. Materials

2,4-dinitrophenylhydrazine (DNPH), 5,5′-dithiobis (2-nitrobenzoic acid) (DNTB), 1-Aniline naphthalene-8-nitrobenzoate (ANS), and fluorescein isothiocyanate (FITC) were purchased from Aladdin Co., Ltd. (Shanghai, China), and Nile red was bought from Shanghai Yuanye Biotechnology Co., Ltd. (Shanghai, China). All other reagents were of analytical grade unless otherwise specified.

2.2. Preparation of CG

Wenye No.2 coconut (Malayan Yellowis coconut population bred by coconut research institute of Chinese academy of tropical agricultural sciences) obtained from Coconut Planting Base in Wenchang city of Hainan Province. The CG was extracted by the modified Patil et al. (2017) method. Briefly, coconuts were hulled, peeled, and dehydrated to collect the coconut meat. In general, coconut meat includes about 4% protein and 40% fat (Yalegama, Nedra Karunaratne, Sivakanesan, & Jayasekara, 2013). Grated coconut meat was freeze-dried and then ground in a grinder to a fine powder. The powder was degreased with hexane using a substance/solvent ratio of 1:10 (w/v) for 2 h. The step was repeated twice to degrease thoroughly, and then the hexane was removed. The powder was mixed with 0.5 mol/L NaCl (a powder-to-solvent ratio of 1:10, w/v) and stirred for 4 h. The supernatant was extracted after centrifugation at 10,000 g for 20 min at 4 °C. The obtained solution was dialyzed (cut-off molecular weight of 10 kDa) for 24 h at 4 °C. Finally, the solution was freeze-dried and stored at 4 °C.

2.3. Preparation of CG treated by ACP

The CG was dissolved in phosphate-buffered saline (PBS, 10 mmol/L, pH 6.8), and adjusted to a final concentration of 5 mg/mL. The prepared CG solution (20 mL) was placed into a polypropylene food tray (180 mm × 150 mm × 50 mm) and treated by an ACP machine (BK-130, Phenix Technologies, USA). The treatment power was set at 50 kV, 60 kV, and 70 kV, and the treatment time was 0 (control), 30, 60, and 90 s. The CG solutions were stored at 4 °C for 12 h until subsequent analysis.

2.4. Sodium dodecyl sulfate-polyacrylamide gel electrophoresis (SDS-PAGE)

The concentrated and separating gels were prepared using 5% and 12% of acrylamide, respectively. The CG samples (50 μL) were diluted and mixed with 5 × loading buffer to reach a concentration of 5 mg/mL. The solution was heated in a boiling water bath for 5 min. Then the processed solution was dissolved in pH 8.3 buffer composed of 50 mmol/L Tris-HCl, 384 mmol/mL glycerol, and 1% SDS in a centrifuge tube. Then, a 10 μL buffer solution containing the proteins was loaded onto a prepared gel. The gel sheets were stained with 2 mg/mL Coomassie Brilliant Blue R-250 for 30 min and destained in a destaining solution (10% methanol and 10% acetic acid).

2.5. Intrinsic fluorescence

The protein samples (10 mL) were diluted to 1 mg/mL in PBS (10 mmol/L, pH 6.8) before measurements. Fluorescence spectra were recorded from 300 to 450 nm with an excitation wavelength of 280 nm by using an F7000 fluorescence spectrophotometer (HITACHI, Tokyo, Japan).

2.6. Protein solubility

The soluble CP content was expressed based on the Bradford method with some modifications (Bradford, 1976). An aliquot in each sample (5 mL, 5 mg/mL) was centrifuged at 10,000 g for 20 min at 4 °C. The Solubility was calculated as the protein concentration ratio in the supernatant after centrifugation to protein concentration before centrifugation.

2.7. Carbonyl, free –SH and S–S bond content

The carbonyl content was measured by the DNPH method with slight modifications (Özaslan & İbanoğlu, 2022). Briefly, 1 mL of protein solution (5 mg/mL) was mixed with 3 mL of DNPH (10 mmol/L), and the mixtures were incubated at 25 °C for 2 h. Subsequently, 4 mL of 20% (v/v) trichloroacetic acid (TCA) was added to stop the reaction. After standing for 20 min, the mixture was centrifuged at 12,000 g at 4 °C for 5 min. After discarding the supernatant, the precipitate pellets were washed three times with 3 mL of ethanol/ethyl acetate solution (1:1, v/v). Then, the final precipitates were redissolved with 3 mL of 6 mol/L active ingredient hydrochloride and centrifuged at 12,000 g for 5 min at 4 °C. The supernatant was taken at 370 nm to measure the absorbance with a UV spectrophotometer (TU-1901, Universal Instruments, Beijing). The carbonyl content was calculated with an extinction coefficient of 22,000 M^{-1} cm^{-1}, and the results were expressed in nmol/mg protein.

The free –SH content and the S–S bond content were determined using DNTB colorimetric method with slight modifications (Zhao, Hong, Fan, Liu, & Li, 2022). To determine the free –SH content, protein solu-tion (1 mL, 5 mg/mL) was mixed with Tris-Glycine-Sodium dodecyl sulfate (Tris-Gly-SDS, 2 mL, 0.1 mg/mL) and Ellman's solution (0.5 mL), and the mixed solution was shake-cultured for 1 h. The absorbance of the solution was determined at 412 nm. The free –SH content was calculated using the extinction coefficient of 13,600 M^{-1} cm^{-1}, and the results were expressed as nmol/mg protein. To determine the S–S bond content, protein solution (2 mL, 5 mg/mL) was mixed with β-mercap-toethanol (0.1 mL) and urea active ingredient hydrochloride (4.0 mL, 6 mol/L urea, 6 mol/L active ingredient hydrochloride), and reacted at 25 °C for 1 h. After adding 10 mL of 12% TCA for 1.0 h, the solution was centrifuged at

10,000 g for 10 min. Then, the precipitate was dissolved in Tris-Gly-SDS buffer (10 mL, 0.1 mg/mL). After Ellman's solution (0.5 mL) was added, the absorbance at 412 nm was measured to calculate the total –SH content. The S–S bond contents were calculated by the following formula (Dong et al., 2017):

$$S-S \text{ bond content (nmol / mg protein)} = \frac{1}{2} \times (\text{total} - \text{SH content} - \text{free} - \text{SH content}) \quad (1)$$

2.8. Circular dichroism (CD) spectrum

CD spectra were recorded on a Bio-Logic MOS-500 circular dichroism spectrometer (Isere, France) in the range of 190–250 nm. The CG solution (10 mL) was diluted to 0.1 mg/mL, and PBS without adding proteins was used as the control. Each sample was collected three times on a silica cuvette with a 0.1 cm path length.

2.9. Fourier transform infrared (FTIR) spectroscopic

The freeze-dried CG powder (100 mg) was pressed into tablets with KBr (1:100, w/w). Subsequently, the FTIR spectra were recorded by an FTIR spectrometer (TENSOR 27, Bruker, Germany) in the wavenumber of 4000-400 cm^{-1}. Each test was a superposition of 32 scans, and the air was used as the background. The secondary structure content of CG was obtained by analyzing the spectra in the range of 1700-1600 cm^{-1} using PeakFit v4.12 software (SeaSolve Software Inc., CA, USA).

2.10. Measurement of particle size distribution and zeta potential

The particle size distribution and zeta potential of CG (10 mL, 0.5 mg/mL) were determined by a Malvern ZS 90 (Malvern Instruments, Malvern, Worcestershire, UK). All experiments were equilibrated for 120 s before measurement and performed three times at 25 °C.

2.11. Surface hydrophobicity (H_0) optimization

H_0 measurement was carried out as described by our previous method (Chen et al., 2020). The protein samples with appropriate serial concentrations were labelled with ANS fluorescent probe, and the fluorescence intensity was collected by an F-7000 spectrofluorometer (Hitachi, Japan). The slope of the fluorescence intensity curve versus protein concentration was used to evaluate H_0.

2.12. Measurement of dynamic interfacial tension

The dynamic interfacial tension was conducted by employing a tensiometer (OT100, Ningbo NB Scientific Instruments, China) with the method of droplet shape analysis. The volume of each droplet was maintained at 10 μL with a protein concentration of 5 mg/mL. The measurement of the dynamic interfacial tension lasted for 60 min until the interfacial tension did not change.

2.13. Preparation of CG-stabilized O/W emulsion

After adding 5 mL of soybean oil to the CG solution (45 mL, 5 mg/mL), the resulting mixture was placed into an Ultra-Turrax (IKA-25, Staufen, Germany) at 10,000 rpm for 1 min. Subsequently, the mixture was further homogenized by using a NanoGenizer30k microfluidic homogenizer (Genizer LLC, CA, USA) at 12,000 psi, and circled once.

2.14. Determination of droplet size

The droplet size of the emulsion was measured using a Mastersizer 3000 (Malvern Instruments, Malvern, Worcestershire, UK) laser particle size analyzer. The refractive index of oil was 1.476, and the refractive index of water was 1.333.

2.15. Characterization of the microstructure of emulsion

The emulsion microstructure was characterized using a Leica TCS SP8 confocal laser scanning microscope (CLSM, Leica Microsystems GmbH, Wetzlar, Germany). Emulsions (10 mL) were mixed with Nile red (50 μL, 0.1 mg/mL) and FITC (200 μL, 0.1 mg/mL) for 30 min. Nile red and FITC were excited using a laser at 488 and 514 nm, respectively.

2.16. Determination of viscosity of the emulsion

The apparent viscosity measurement using a rheometer (MCR302, Anton-Paar, Ostfildern, Germany). The shear rate was increased from 1 to 100 s^{-1}, and the constant frequency was set at 1 Hz.

2.17. Storage stability of the emulsion

The fresh emulsion (25 mL) was placed in glass test tubes with 0.2 mg/mL sodium azide at 4 °C. The droplet sizes of the emulsions were determined at 2, 4, 6, 8, and 10 d.

2.18. Centrifugal stability of the emulsion

The stabilization behaviors of the emulsion were further evaluated by an optical analytical centrifuge (LUMiSizer, L.U.M. GmbH, Germany). The instrumental parameters for the measurement were set as follows: temperature, 25 °C; rotational speed, 4000 r/min; time interval, 10 s; total experiment time, 50 min. The transmission profile of the sample tube was recorded with increasing separation time. Each experiment (0.550 mL of emulsion) was conducted in triplicate. The instability index and integral transmission were analyzed by SEPView software (LUM GmbH, Berlin, Germany).

2.19. Statistical analysis

Data were analyzed by the software package SPSS 24.0 (SPSS Inc., Chicago, USA). One-way ANOVA and Duncan factorial scheme were adopted for statistical analysis. Differences were considered to be significant with $p < 0.05$.

3. Results and discussion

3.1. Effect of the ACP treatment on SDS-PAGE of CG

The gel electrophoresis method using SDS-PAGE to determine the molecular weights of proteins is presented in Fig. 1a. CG is composed mainly of 11S globulin (326 kDa) and a small amount of 7S globulin (Patil et al., 2017). In the native state, 11S globulin, with a molecular weight of 326 kDa, resolves into two main bands at 23 and 32 kDa (Laurena & Tecson-Mendoza, 2005). Furthermore, the band at 55 kDa is a recombination of both bands. 7S globulin, with a molecular weight of 156 kDa in the native state, resolves in a set of distinct bands at 16, 22,

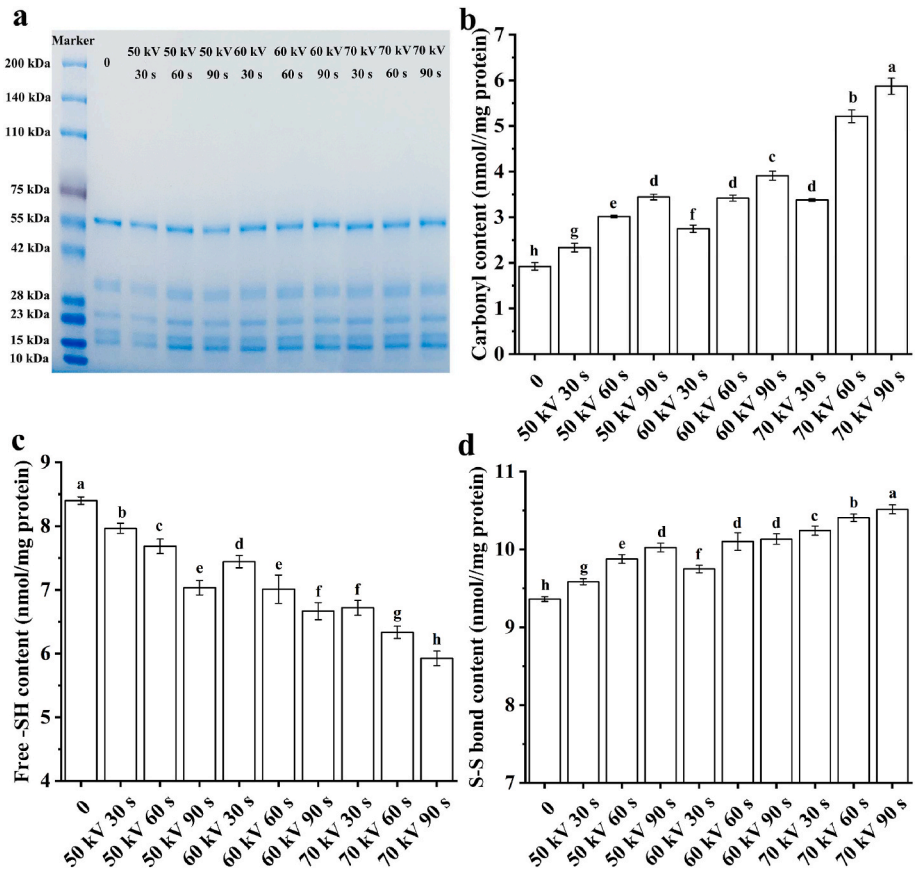

Fig. 1. SDS-PAGE (a), carbonyl content (b), free –SH content (c), and S–S bond content (d) of coconut globulin after atmospheric pressure cold plasma treatment at 50, 60, and 70 kV for 0, 30, 60, and 90 s. Different lowercase letters indicate significant differences ($p < 0.05$).

and 24 kDa subunits (Chambal, Bergenståhl, & Dejmek, 2012). The high-energy particles produced by the ACP treatment could bombard the covalent bonds of CG to form subunits of small molecular weight (Ji et al., 2020). The bands of CG did not change significantly after ACP treatment at 50 kV 30 s, indicating that the degradation of CG molecules by ACP was slight. After the ACP treatment at 50 kV and 60 kV for 60 and 90 s, the CG band at 55 kDa became lighter, and the corresponding small molecular weight band deepened, indicating the degradation of the 11S subunit. During the interaction between ACP and liquid, free radicals were produced, which could affect the structure of the protein, including cleavage of covalent bonds, interaction with amino acids, and modification of side groups (Xu et al., 2021). The decrease in CG molecular weight might be the result of various free radicals acting on covalent bonds together. However, the disulfide bonds generated by high-strength ACP treatment could cause the aggregation of protein molecules (Sharma & Singh, 2022). All CG bands at 55 kDa deepened after the ACP treatment at 70 kV, which might be due to the formation of disulfide bonds that induced intermolecular aggregation. The results of SDS-PAGE indicated that moderate ACP treatment could lead to covalent bond breaking and macromolecular degradation of CG molecules, while excessive ACP treatment could cause intermolecular aggregation.

3.2. Effect of the ACP treatment on the degree of CG oxidation

Protein oxidation, initiated by free radicals, can be measured by the loss of free –SH groups, formation of S–S bonds, or formation of protein carbonyls (Wang, Zhou, Zhou, Tu, & Xu, 2022). Free radicals can result in the scission of the peptide backbone, conversion of one amino acid to a different amino acid, formation of cross-links, and oxidative changes in amino acid side chains (Zhang et al., 2021). Therefore, the carbonyl content, free –SH content, and S–S bond content of CG after the ACP treatment were determined as shown in Fig. 1b–d.

As shown in Fig. 1b, ACP-treated CG had higher protein carbonyl content than untreated CG ($p < 0.05$). Simultaneously, the increase in carbonyl formation content was the plasma voltage and treatment time-dependent, especially at 70 kV 90 s (the CG carbonyl content was 5.87 nmol/mg protein). These phenomena might be that the amino acid side chains, such as those with –NH or $–NH_2$ groups, were oxidized by the reactive species of ACP, especially hydroxyl radicals and ozone (Zhou et al., 2016). These results were in good agreement with that the carbonyl content of ACP-treated protein (whey protein and squid skin protein) increased (Nyaisaba et al., 2019a, 2019b).

In addition, the modification by ACP also induces some changes in the side chains of sulfur-containing amino acids. CG significantly decreased the free –SH groups after the ACP treatment, which was significantly influenced by treatment time and voltage ($p < 0.05$). Simultaneously, it was observed that the ACP treatment promoted the S–S bond formation of CG. The free –SH group content increased with the increase in treatment time, while the S–S bond content increased. The following aspects could explain these results: (1) the free radicals, combining with the free –SH groups on the surface of CG, produced sulfhydryl radicals, which formed intra or inter-molecular S–S cross-links or were further oxidized into new S–S bonds (Dong et al., 2017); (2) the free radicals oxidized sulfur-containing amino acids, especially cysteine, and reduced free –SH groups by oxidation of thiol groups to S–S bonds.

3.3. Effect of the ACP treatment on the secondary structure of CG

The secondary structure of a protein mainly depends on the arrangement of the amide groups, which are determined by the conformation of the main chain. CD spectra are determined based on the

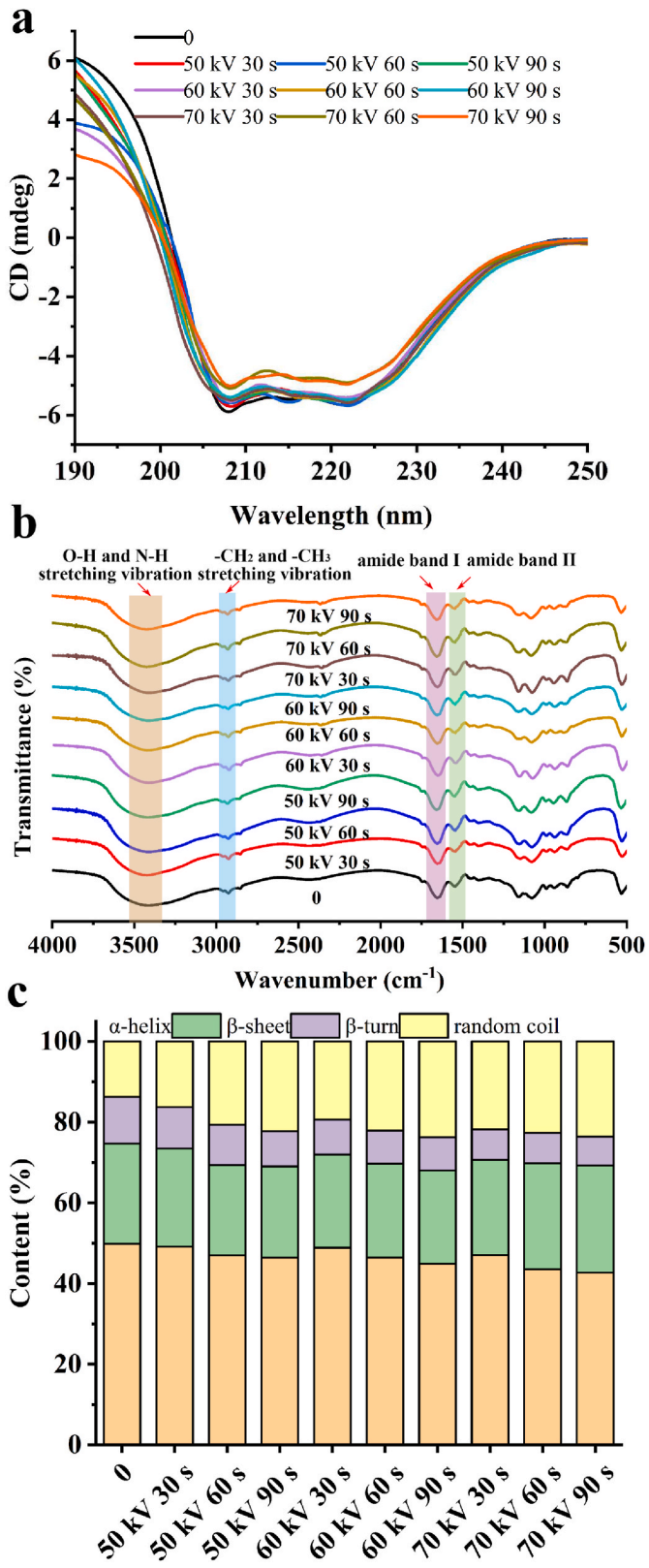

Fig. 2. FTIR spectra (a), CD spectra (b), and secondary structure content (c) of coconut globulin after atmospheric pressure cold plasma treatment at 50, 60, and 70 kV for 0, 30, 60, and 90 s.

secondary structural composition and spatial arrangement of the amide groups (Hu et al., 2021). In CD spectra, two negative double-humped bands at 208 and 222 nm, produced by peptide bond π→π* and n→π* transitions, are the typical characteristics of α-helices (Rahmani-Manglano et al., 2022). The CD spectra curves of CG treated with ACP under different conditions are shown in Fig. 2. The broad negative bands exhibited by CG around 208 and 222 nm corresponded to its secondary structure of α-helix. It was observed that the decrease in negative ellipticities in the two peaks demonstrated the reduction in the α-helix content of CG after the ACP treatment in Fig. 2a. These results suggested that the ACP treatment disrupted the spherical structure of CG molecules into a looser structure, which was dominated by ordered structure and transformed into the partially disordered structure.

FTIR spectra are also a common method to study the secondary structure of proteins. The peaks at 1700-1600 cm^{-1} and 1600-1500 cm^{-1} represent the spectral features of amide bands I and II, respectively (Hao et al., 2022). The amide I bands are mainly attributed to the C═O stretching vibration of the carbonyl group (Ren et al., 2022). The amide II bands are ascribed to the bending vibrations of the N–H groups and the stretching vibrations of the C–N groups (Nooshkam, Varidi, & Alkobeisi, 2022). Amide bands I and II are commend used to characterize the change of protein secondary structures due to their vibration frequency's sensitivity to protein conformation (Yang et al., 2022). It was observed that FTIR spectra of CG were significantly changed in these two regions after the ACP treatment, implying changes in the secondary structure of the protein. Furthermore, the broadband at 3500-3100 cm^{-1} was attributed to the O–H and N–H stretching vibrations of the hydroxyl/amino groups of CG. After the ACP treatment, this peak of CG shifted to the larger wavenumbers, especially at 70 kV 90 s. The unfolding of protein structures, caused by free radicals, provided more binding sites for hydrogen bonds, promoting the formation of intermolecular and intramolecular hydrogen bonds (Li, Yang, et al., 2022). In addition, CG exhibited multiple peaks at 3000-2750 cm^{-1}, which corresponded to the symmetric and asymmetric stretching vibrations of $–CH_2$ and $–CH_3$ at different positions (Li, Huang, et al., 2022). After ACP treatment, a slight shift was observed, which might be the destruction of CG side chain amino acids by free radicals (Yuan, Liu, & Liu, 2015).

The Fourier self-deconvolution method was further used to fit the FTIR spectra in the range of 1700-1600 cm^{-1} to acquire the content of the secondary structure in CG. As shown in Fig. 2c, the native CG contained 49.85% α-helix, 24.82% β-sheet, 11.62% β-turn and 13.70% random coil. After the ACP treatment, the content of α-helix and β-turn of CG decreased, while the content of random coil increased. These changes suggested that the ACP treatment led to the deconstruction and unfolding of CG secondary structure, promoting the transformation of α-helix and β-turn to random coil structure.

3.4. *Effect of the ACP treatment on the intrinsic fluorescence of CG*

The intrinsic fluorescence of a protein, which is mainly attributed to tryptophan (Trp), tyrosine (Tyr), and phenylalanine (Phe) residues, is very sensitive to the changes in the microenvironment surrounding these residues (Lei et al., 2022). Thus, the intrinsic fluorescence spectra were analyzed by analyzing precise differences in fluorescence intensities and spectral profiles to account for changes in protein tertiary structure (Huang et al., 2022). As depicted in Fig. 3a, the fluorescence intensity of CG is gradually quenched with increasing time and voltage of the ACP treatment. A slight blue shift of the emission maximum peak of CG was observed, indicating that the conformation of the CG molecule was changed after the ACP treatment. In addition, the microenvironment around Trp, Tyr, and Phe residues might change from hydrophobic to hydrophilic. Fig. 3b–d are used to compare the effect of the ACP treatment time on the CG structure at the same voltage. It was observed that the decrease in fluorescence intensity after the ACP treatment indicated that the local environment of hydrophobic residues became more polar (Li et al., 2017). In conclusion, these results suggested the

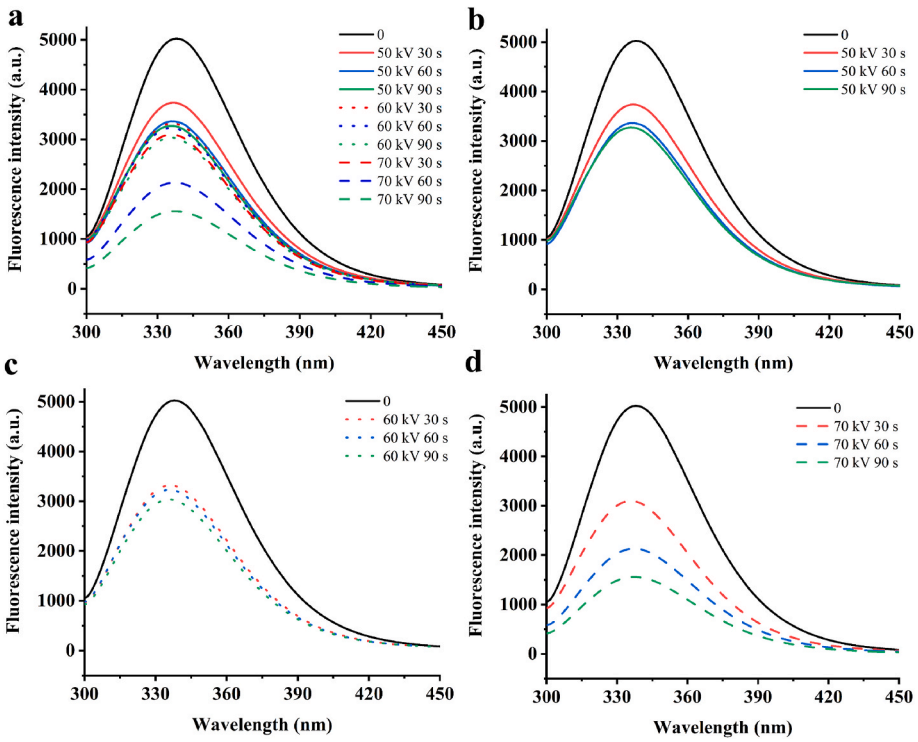

Fig. 3. Fluorescence emission spectra of coconut globulin after atmospheric pressure cold plasma treatment at 50, 60, and 70 kV for 0, 30, 60, and 90 s (a), fluorescence emission spectra of coconut globulin after atmospheric pressure cold plasma treatment at 50 (b), 60 (c), and 70 kV (d) for 0, 30, 60, and 90 s.

ACP treatment-induced unfolding of CG and exposure of hydrophobic groups. The conformational changes of CG might affect its adsorption on the oil-water interface, thereby influencing the emulsifying properties.

3.5. Effect of the ACP treatment on the particle size distribution, average particle size, zeta potential and solubility of CG

After the ACP treatment, the particle size distribution, average particle size, and zeta potential of CG are shown in Fig. 4. At 50 kV and 60 kV, the particle size distribution showed a trend of decreasing size with the increase of the ACP treatment time in Fig. 4b and c. At the same time, the distribution curve showed a narrower and sharper peak after the ACP treatment, indicating that the particle sizes of the CG solution were more uniform. This was related to the increase in the absolute value of the zeta potential after the ACP treatment, increasing the repulsive force between CG molecules. The high surface charges can provide larger intermolecular electrostatic repulsion for colloidal particles, thus reducing the formation of aggregates caused by intermolecular attraction (Bhattacharjee, 2016). A moderate modification was beneficial to the reduction of particle size of CG, especially 60 kV 60 s (207.63 nm) and 60 kV 90 s (204.20 nm). However, when over-modified at 70 kV, the structural unfolding of CG promoted the exposure of hydrophobic groups to the surface, which promoted protein-protein interactions and aggregation. Therefore, the particle sizes of CG increased after the ACP treatment at 70 kV and were still smaller than that of untreated CG (440.56 nm). These results were consistent with Dong et al. (2017). The changes in the zeta potential of CG after the ACP treatment are shown in Fig. 4f. At 50 kV and 60 kV, the absolute values of zeta potential enhanced significantly as the treatment time increased, which was that free radicals could promote the formation of polar charges on the surface of CG (Sun et al., 2021). After the ACP treatment at 70 kV, the absolute values of the zeta potential of CG decreased and were still higher than that of untreated CG (−14.1 mV). The result was that over-modified CG molecules aggregated, leading to the shielding of charged groups on the protein surface.

Solubility, one of the most important characteristics of proteins, can influence other functional properties (Gao, Rao, & Chen, 2022). The concentration of soluble CG was maximum at 60 kV 60 s and 60 kV 90 s, with a small decrease observed at 70 kV (Fig. 5a). The increase in the solubility of CG might be due to the increased exposure of protein surface-charged groups to water molecules activated by the ACP treatment. The ACP treatment increased the structure irregularity of CG, which could expose more charged groups to reduce intermolecular aggregation and provide more binding sites for water molecules (Sadeghi, Koocheki, & Shahidi, 2021). As excessive modification (70 kV), the decrease of CG solubility might be due to overcrowding of protein micelles at the active site, which reduced the number of active sites and reduced solubility (Dong, Gao, Xu, & Chen, 2016).

3.6. Effect of the ACP treatment on surface properties of CG

To explore the mechanism between physicochemical properties and emulsifying properties, surface property indexes (H_0 and interfacial tension) of CG were measured. The results are shown in Fig. 5b.

The H_0 of CG was used to reflect the aggregation tendency of CG molecules and the number of hydrophobic groups on the surface of a protein. In the native state, the CG molecules, with hydrophobic groups buried inside the protein, exhibited low H_0. Correspondingly, the H_0 values increased gradually with time at 50 kV and 60 kV. The H_0 values showed the highest value at 60 kV 60 s and 60 kV 90 s. Moderate modification can induce structural unfolding and fragmentation of proteins, which improved the exposure of amino acids and accessibility to the binding sites (Baek et al., 2021). Interestingly, compared to the time, the voltage was more sensitive to H_0. However, at higher voltage treatment (70 kV), exposure to excessive hydrophobic residues enhanced protein-protein interactions, leading to protein aggregation (particle size increased in Fig. 4).

The adsorption of protein at the oil-water interface is a dynamic process: (1) positioning at the oil-water interface. The hydrophobic group of protein points to the oil phase and the hydrophilic group points

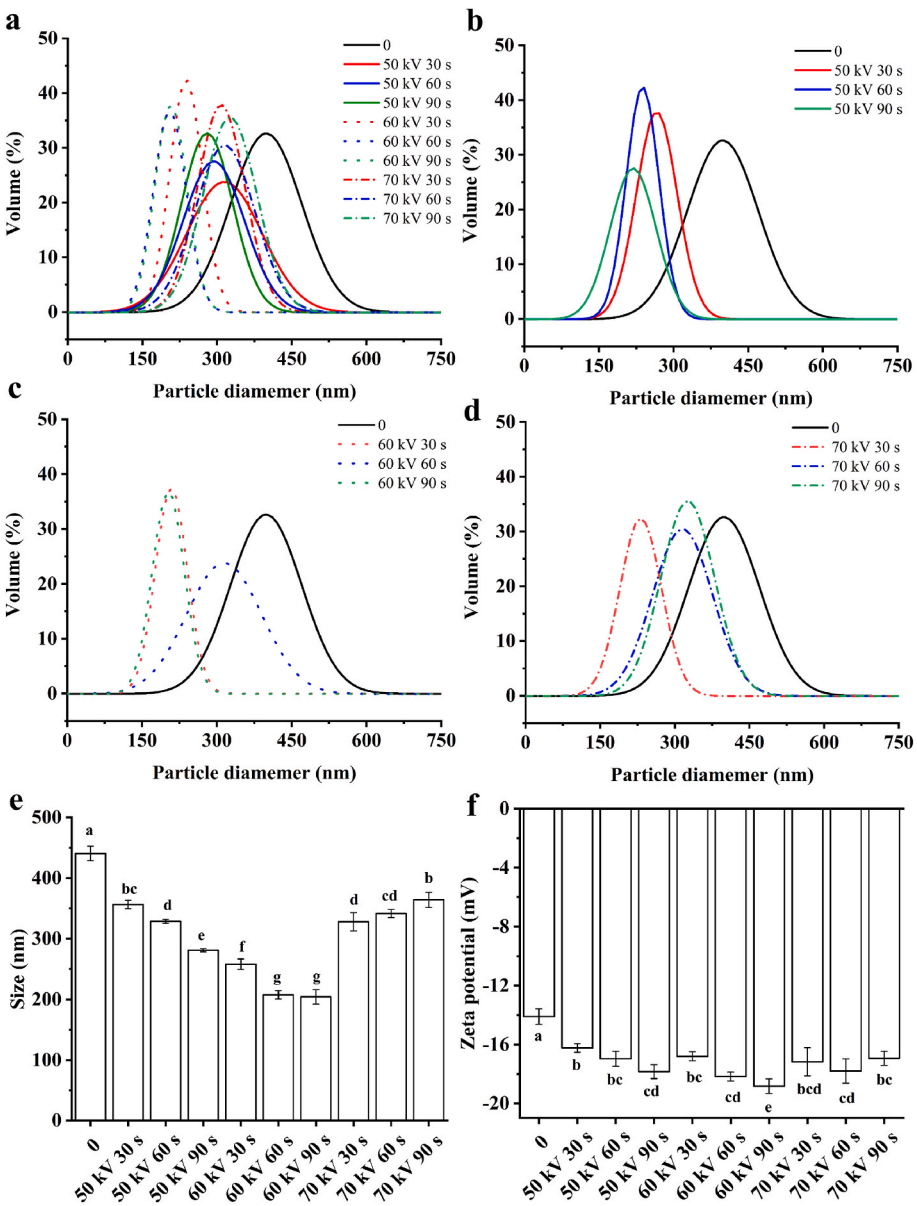

Fig. 4. Particle size distribution of coconut globulin after atmospheric pressure cold plasma treatment at 50, 60, and 70 kV for 0, 30, 60, and 90 s (a), particle size distribution of coconut globulin after atmospheric pressure cold plasma treatment at 50 (b), 60 (c) and 70 kV (d) for 0, 30, 60 and 90 s, particle size (e) and zeta potential (f) of coconut globulin after atmospheric pressure cold plasma treatment at 50, 60 and 70 kV for 0, 30, 60 and 90 s. Different lowercase letters indicate significant differences ($p < 0.05$).

to the water phase; (2) denaturation of protein molecules. Buried hydrophobic groups exposed on the surface; (3) rearrangement of proteins at the oil-water interface (Zhou, Tobin, Drusch, & Hogan, 2021). Therefore, the dynamic interfacial tension of CG at the oil-water interface was determined in a time-dependent manner (Fig. 5c). It was found that the interfacial tension first decreased rapidly, corresponding to protein adsorption. Subsequently, this was a slow evolution of interfacial tension with time, corresponding to the rearrangement of proteins. The interfacial tension value of native CG was 13.61 mN/m after 3600 s. That was related to that the more hydrophilic character of CG prevented the CG molecules to adsorb to the polar oil/water interface in a small amount due to the relatively weak intermolecular interactions between the protein and oil. After the ACP treatment, the interface tension of CG decreased, indicating that the ACP treatment improved the interfacial activity of CG and increased the interfacial adsorption (Wan et al., 2014). This phenomenon was explained by the fact that the free radicals by the ACP treatment induced the changes in CG structure or introduced new groups, which greatly promoted the adsorption of CG on the interface. Nevertheless, over-modified CG molecules, with higher particle sizes (ACP treated at 70 kV), were less prone to efficiently accommodate at the oil/water interface.

3.7. Effect of the ACP treatment on the emulsifying ability of CG

Emulsifying activity, a crucial property of proteins, is affected by many factors, such as structural stability, surface hydrophobicity, and molecular flexibility. The emulsifying activity was determined by measuring the droplet size of the emulsion, which was represented by $D_{4,3}$ as shown in Fig. 6a. In general, the ideal emulsifying activity exhibits emulsion droplets with small particle sizes and uniform distribution. The untreated CG-stabilized emulsion showed a larger droplet size (23.67 μm), which was related to the easier aggregation of droplets under the influence of weak electrostatic repulsion. The poor-modified CG (50 kV 30 s) and the over-modified CG (70 kV 60 s and 70 kV 90 s) were 21.13 μm, 21.57 μm and 22.36 μm, respectively, which were not significantly different from the untreated group ($p > 0.05$). Simultaneously, the emulsion state appeared as delamination, which was an unstable state. These results could be explained by the formation of aggregates between amino acid chains (Sharifian, Soltanizadeh, & Abbaszadeh, 2019). Interestingly, the moderate-modified CG (60 kV 60

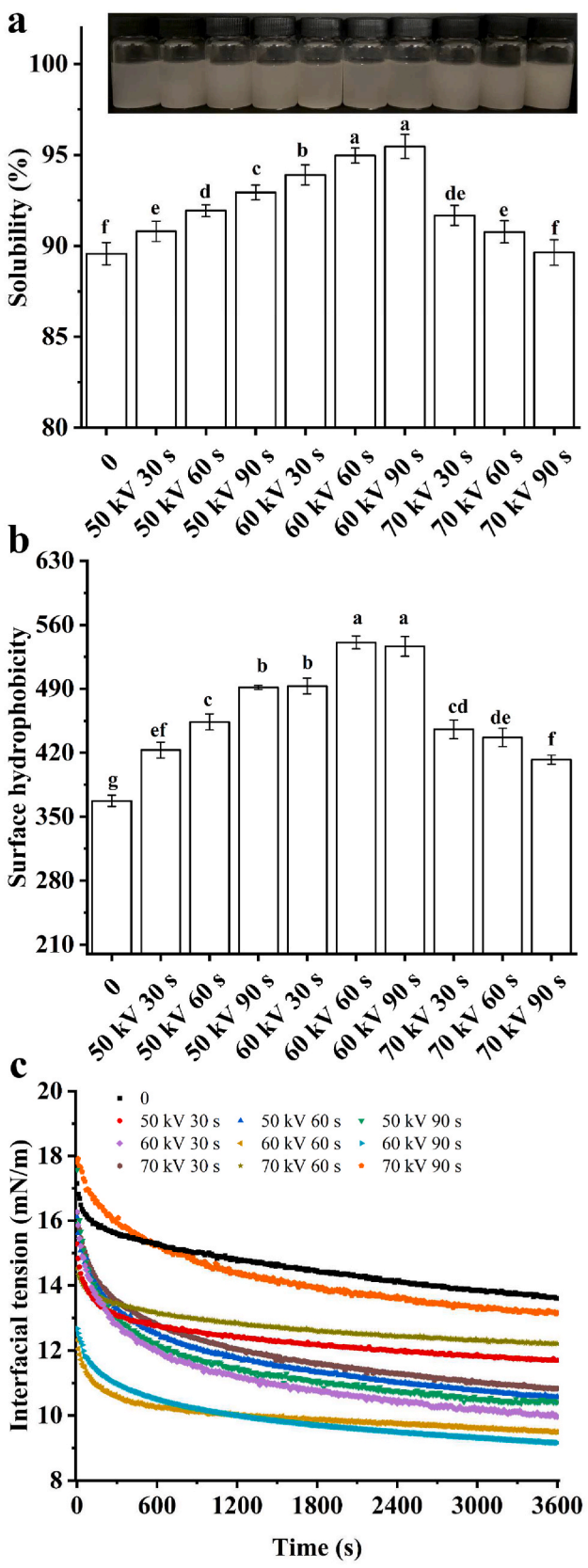

Fig. 5. Solubility (a), surface hydrophobicity (b), and dynamic interfacial tension (c) of coconut globulin after atmospheric pressure cold plasma treatment at 50, 60, and 70 kV for 0, 30, 60, and 90 s. Different lowercase letters indicate significant differences ($p < 0.05$).

s) stabilized emulsion was small in droplet size (14.73 μm) and did not delaminate, suggesting that the ACP treatment might be a potential method for physically modifying proteins. As mentioned before, free radicals generated by the ACP treatment broke the intermolecular bonds of CG, promoted the change of protein conformation at the interface, and reduced the interfacial tension.

The morphology of the microstructure of the emulsion stabilized by CG with different ACP treatments was investigated using CLSM, and the images are presented in Fig. 6b. A hybrid dye solution was integrated into the system, with 0.1 mg/mL Nile red added to the oil phase and 0.1 mg/mL FITC mixed with the CG molecules. The oil phase was shown in green and the water phase was shown in red. It was observed that all emulsions were spherical droplets with oil droplets on the inside and protein on the outside, implying O/W emulsion. Interestingly, the oil droplets were dispersed homogeneously with a decreased particle size with an increase of the ACP treatment time from 0 to 90 s at 50 kV or 60 kV. However, larger oil droplets appeared in the images with increasing inhomogeneity of droplet dispersion at 70 kV 60 s and 70 kV 90 s (Fig. 6b). Moreover, the distribution of oil droplets was relatively dense, which might be due to the increase in the amount of protein adsorbed on the surface of oil droplets at 60 kV 60 s and at 60 kV 90 s (Hu et al., 2022).

Rheological property is considered one of the important indicators of emulsion properties, which is affected by protein structure and interaction between droplets. Changes in viscosities as a function of shear rates of emulsions stabilized by CG are presented in Fig. 6c. The viscosity of all emulsions decreased as the shear rate increased, showing pseudoplastic behavior. As the shear rate increases, the emulsion droplets became more ordered under Brownian motion (Giuntoli, Puosi, Leporini, Starr, & Douglas, 2020). It was worth noting that the emulsions stabilized by CG had higher viscosity at 60 kV 60 s and 60 kV 90 s. After the ACP treatment, interfacial protein interactions (polymerization and cross-linking) were stronger, which promoted the formation of films with higher viscoelasticity (Misra, Yong, Phalak, & Jo, 2018). In addition, the apparent viscosity also depended on the ACP treatment time and voltage, which was related to the degree of CG molecular structure change after the ACP treatment.

In conclusion, the effect of the ACP treatment on the emulsifying ability of CG was dependent on treatment time and voltage. CG and untreated CG exhibited similar emulsifying abilities when poor modification (50 kV 30 s) and excessive modification (70 kV 60 s and 70 kV 90 s). Notably, when moderately modified (60 kV 60 s and 60 kV 90 s), the CG molecular structure unfolded properly, which effectively reduced the interfacial tension and improved the emulsifying ability.

3.8. *Effect of the ACP treatment on emulsion stability of CG*

Emulsions are prone to instability over-processing due to various physicochemical mechanisms, including flocculation, coalescence, gravity separation, Ostwald ripening, and phase inversion (Degner, Chung, Schlegel, Hutkins, & McClements, 2014). Therefore, the emulsion storage stability and centrifugation stability were analyzed as shown in Figs. 7 and 8.

The droplet sizes of CG-stabilized emulsion are analyzed in Fig. 7a during 0, 2, 4, 6, 8, and 10 d after the ACP treatment. All droplet sizes increased with storage time, indicating that oil molecules grew at the expense of small oil droplets by diffusing through the intermediate aqueous phase. After 10 d, the droplet sizes of the emulsions were drastically higher than their initial values, which was due to coalescence and Ostwald ripening (Yang et al., 2021). Droplet size changes of emulsions during storage were closely related to the ACP treatment time and voltage. After the ACP treatment at 60 kV, especially for 60 s, the CG-stabilized emulsions exhibited smaller droplet sizes throughout the storage period. This indicated that CG could be adsorbed and retained at the oil-water interface for a long time after moderate modification by the ACP treatment, thus resisting the destabilization of the emulsion during

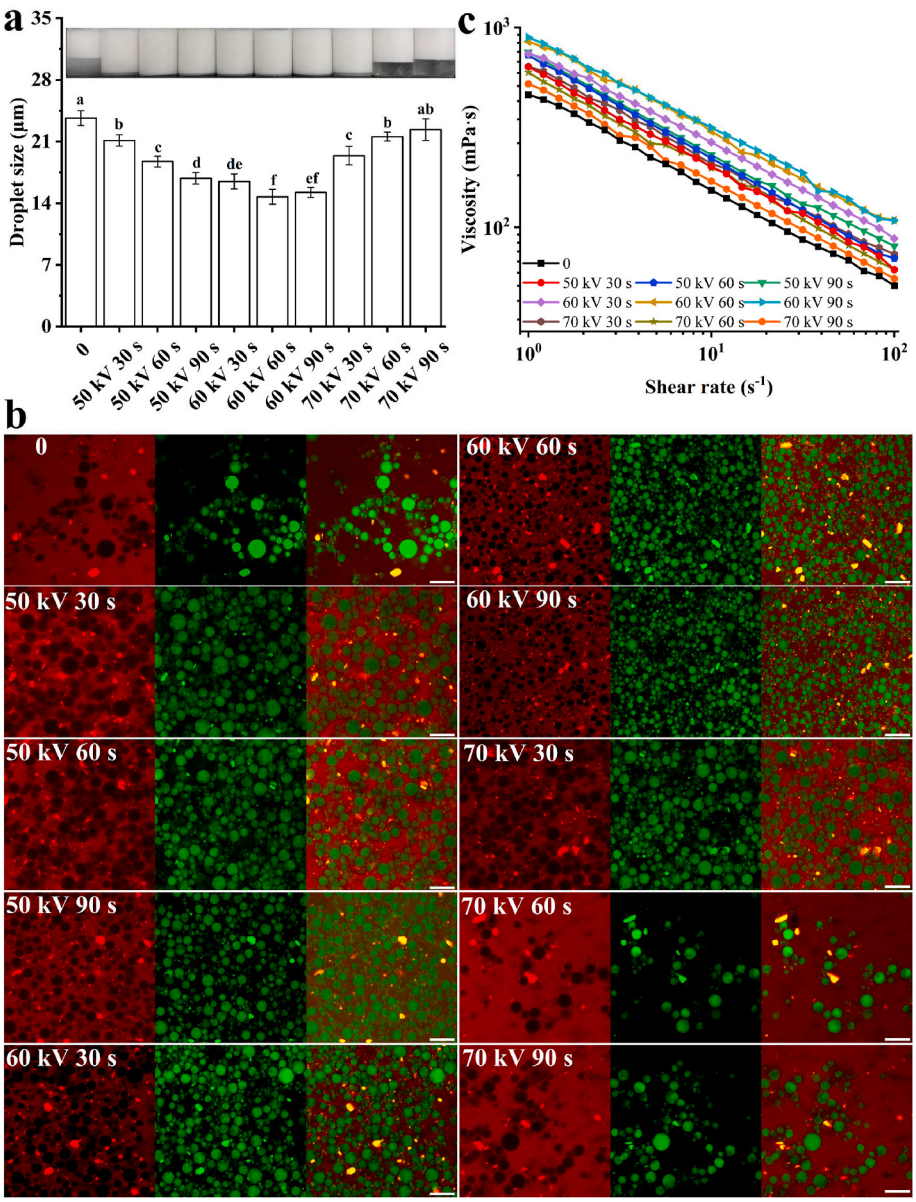

Fig. 6. Droplet size (a), CLSM images (b), and viscosity (c) of emulsion stabilized by coconut globulin after atmospheric pressure cold plasma treatment at 50, 60, and 70 kV for 0, 30, 60, and 90 s. Scale bars, 30 μm. Different lowercase letters indicate significant differences ($p < 0.05$).

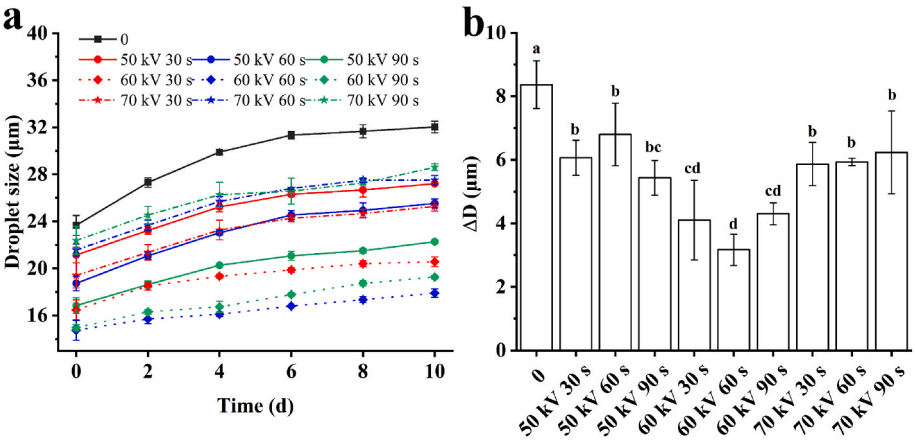

Fig. 7. Droplet size (a) and ΔD (the tenth-day droplet size - the fresh droplet size) (b) of emulsion stabilized by coconut globulin during 0, 2, 4, 6, 8, and 10 d after atmospheric pressure cold plasma treatment at 50, 60, and 70 kV for 0, 30, 60, and 90 s. Different lowercase letters indicate significant differences ($p < 0.05$).

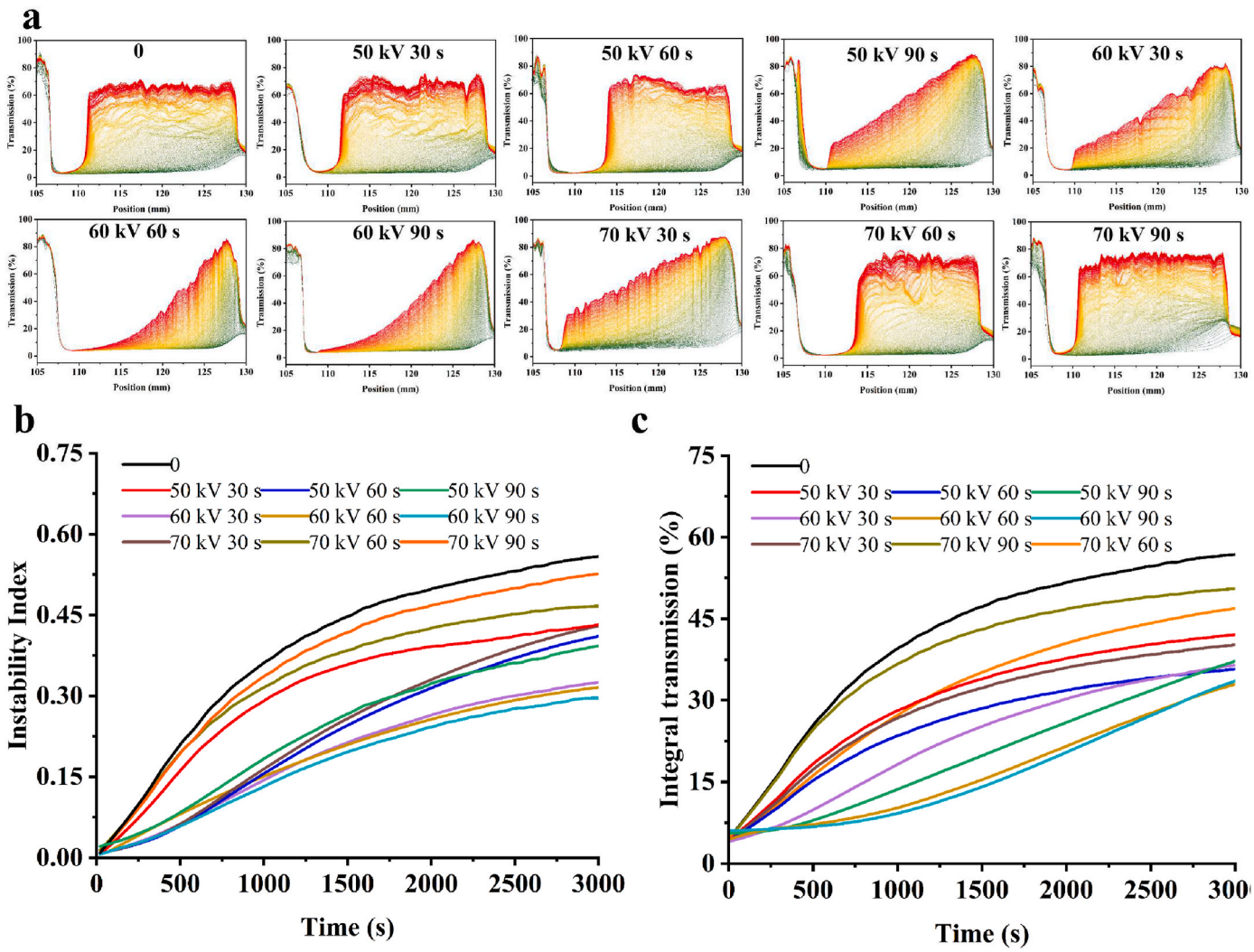

Fig. 8. Transmission profile (a), instability index(b), and integral transmission (c) of emulsion stabilized by coconut globulin after atmospheric pressure cold plasma treatment at 50, 60, and 70 kV for 0, 30, 60, and 90 s.

storage. Fig. 7b further quantifies droplet size changes during emulsion storage. ΔD represented the difference between the tenth-day droplet size and the fresh droplet size. The droplet size changes of the modified CG-stabilized emulsion were all smaller than that of the untreated (8.37 μm) within 10 d. In addition, the ΔD of the emulsions has not significantly different between 50 kV and 70 kV, while the ACP treatment at 60 kV exhibited a smaller ΔD. These results were explained by the following reasons: (1) the absolute values of zeta potential of the moderate-modified CG were larger, which caused a large electrostatic repulsion between the emulsion droplets, thereby hindering the aggregation of the emulsion droplets (Xie et al., 2022); (2) the emulsifier with small particle size (the moderate-modified CG) was helpful to improve the protein coverage at the oil-water interface, thus protecting droplets against coalescence (Zhang et al., 2018).

To further characterize the emulsion stability, the CG-stabilized emulsion stability was evaluated by accelerated centrifugation under different ACP treatment conditions. The LUMiSize stability analyzer represents a time- and space-dependent transfer curve over the entire sample length under centrifugation (Gross-Rother et al., 2018). Initially, the emulsion particles are uniformly distributed throughout the sample. Subsequently, after centrifugation, the emulsion particles move from the meniscus to the bottom of the cuvette. Therefore, the movement of emulsion particles is visualized by transmitted light intensity over time, achieving quantification of emulsion particle instability processes. As shown in Fig. 8a, the bottom green line represented the first transfer profile, and the top red line represented the last transfer profile. Over time during centrifugation, the emulsion became unstable, with lighter oil droplets gradually migrating upward, which led to sedimentation. Therefore, the transmission at the bottom of the sample tube gradually increased, and the transfer profile moved up over time. The smaller the change in transmittance of the sample in the tube (closer to 0 or the smaller the transmission area), the more stable the emulsion was (Zheng et al., 2022). CG-stabilized emulsions were most stable after the ACP treatment (60 kV 60 s and 60 kV 90 s). The instability index and integral transmission over time are also shown in Fig. 8b and c. It was observed that the instability index and integral transmission increased with time, indicating that the emulsion was becoming more and more unstable (Niu, Chen, Luo, Chen, & Fu, 2022). Compared to the control, the instability index and integral transmission of the CG-stabilized emulsion decreased after the ACP treatment, especially at 60 kV 60 s and 60 kV 90 s. This further illustrated that moderate modification could improve the stability of CG-stabilized emulsions.

4. Conclusion

This study investigated the effect of the ACP treatment as a non-thermal sterilization technique on the structure and emulsifying properties of CG. Indeed, the ACP treatment promoted the formation of S–S

bonds and carbonyl groups by breaking the covalent bonds in CG molecules. The ACP treatment induced the secondary structure of CG to be more disordered and promoted the transformation of α-helix and β-turn to random coil structure. The destruction of covalent bonds after the ACP treatment further resulted in a decrease in the degree of aggregation (decrease of particle size) and an increase in the surface charge (enhancement of absolute values of zeta potential) of CG molecules. In particular, moderate modification by the ACP treatment increased the adsorption of CG at the oil-water interface, which was achieved by exposing the hydrophobic groups to a more hydrophilic environment and the enhancement of H_0. Furthermore, the effect of the ACP treatment on emulsifying properties was highly dependent on the treatment conditions (treatment time and voltage). After the moderate ACP treatment (60 kV 60 s and 60 kV 90 s), the droplet sizes of the CG-stabilized emulsion decreased, accompanied by an increase in viscosity and a more uniform droplet distribution. However, the emulsifying properties of CG molecules after poor modification and excessive modification were close to those of untreated. The CG-stabilized emulsions after the moderate ACP treatment also showed better stability, which was manifested in the reduction of droplet aggregation and phase separation during storage and centrifugation. The improvement of CG emulsifying properties was closely related to the modification of its structure by the ACP treatment. Our research provides theoretical bases for the ACP treatment to improve the stability and reduce the use of exogenous emulsifiers in liquid food during sterilization. Our future research direction will focus on the effects of ACP treatment on the shelf life and qualities of coconut milk.

Author statement

Yang Chen: Conceptualization, Methodology, Writing - Original Draft, Writing - Review & Editing, Visualization, Mengying Yao: Methodology, Software, Tianyi Yang: Investigation, Yajing Fang: Investiga-tion, Resources, Dong Xiang: Resources, Supervision, Weimin Zhang: Conceptualization, Formal analysis, Funding acquisition.

Declaration of competing interest

The authors declare that they have no known competing financial interests or personal relationships that could have appeared to influence the work reported in this paper.

Data availability

Data will be made available on request.

Acknowledgement

The authors acknowledge the financial support from the National Natural Science Foundation of China (No. 32260609).

References

Ariyaprakai, S., Limpachoti, T., & Phattayakorn, P. (2015). Interfacial and emulsifying properties of sucrose ester in coconut milk emulsions in comparison with Tween. *Food Hydrocolloids, 30*(1), 358–367. https://doi.org/10.1016/j.foodhyd.2012.06.003

Baek, K. H., Heo, Y. S., Yim, D. G., Lee, Y. E., Kang, T., Kim, H. J., et al. (2021). Influence of atmospheric-pressure cold plasma-induced oxidation on the structure and functional properties of egg white protein. *Innovative Food Science & Emerging Technologies, 74*, Article 102869. https://doi.org/10.1016/j.ifset.2021.102869

Bhattacharjee, S. (2016). DLS and zeta potential - what they are and what they are not? *Journal of Controlled Release, 235*, 337–351. https://doi.org/10.1016/j.jconrel.2016.06.017

Bradford, M. M. (1976). A rapid and sensitive method for the quantitation of microgram quantities of protein utilizing the principle of protein-dye binding. *Analytical Biochemistry, 72*, 248–254. https://doi.org/10.1016/0003-2697(76)90527-3

Chalupa-Krebzdak, S., Long, C. J., & Bohrer, B. M. (2018). Nutrient density and nutritional value of milk and plant-based milk alternatives. *International Dairy Journal, 87*, 84–92. https://doi.org/10.1016/j.idairyj.2018.07.018

Chambal, B., Bergenståhl, B., & Dejmek, P. (2012). Edible proteins from coconut milk press cake; one step alkaline extraction and characterization by electrophoresis and mass spectrometry. *Food Research International, 47*(2), 146–151. https://doi.org/10.1016/j.foodres.2011.04.036

Chen, Y., Li, Z. S., Yi, X. Z., Kuang, H. R., Ding, B. M., & Sun, W. Q. (2020). Influence of carboxymethylcellulose on the interaction between ovalbumin and tannic acid via noncovalent bonds and its effects on emulsifying properties. *LWT - Food Science and Technology, 118*, Article 108778. https://doi.org/10.1016/j.lwt.2019.108778

Coutinho, N. M., Silveira, M. R., Rocha, R. S., Moraes, J., Ferreira, M. V. S., Pimentel, T. C., et al. (2018). Cold plasma processing of milk and dairy products. *Trends in Food Science & Technology, 74*, 56–68. https://doi.org/10.1016/j.tifs.2018.02.008

Degner, B. M., Chung, C., Schlegel, V., Hutkins, R., & McClements, D. J. (2014). Factors influencing the freeze-thaw stability of emulsion-based foods. *Comprehensive Reviews in Food Science and Food Safety, 13*(2), 98–113. https://doi.org/10.1111/1541-4337.12050

Dong, S., Gao, A., Xu, H., & Chen, Y. (2016). Effects of dielectric barrier discharges (DBD) cold plasma treatment on physicochemical and structural properties of zein powders. *Food and Bioprocess Technology, 10*(3), 434–444. https://doi.org/10.1007/s11947-016-1814-y

Dong, S., Wang, J. M., Cheng, L. M., Lu, Y. L., Li, S. H., & Chen, Y. (2017). Behavior of zein in aqueous ethanol under atmospheric pressure cold plasma treatment. *Journal of Agricultural and Food Chemistry, 65*(34), 7352–7360. https://doi.org/10.1021/acs.jafc.7b02205

Gao, K., Rao, J. J., & Chen, B. C. (2022). Unraveling the mechanism by which high intensity ultrasound improves the solubility of commercial pea protein isolates. *Food Hydrocolloids, 131*, Article 107823. https://doi.org/10.1016/j.foodhyd.2022.107823

Giuntoli, A., Puosi, F., Leporini, D., Starr, F., & Douglas, J. F. (2020). Predictive relation for the α-relaxation time of a coarse-grained polymer melt under steady shear. *Science Advances, 6*(17), eaaz0777. https://doi.org/10.1126/sciadv.aaz0777

Gross-Rother, J., Herrmann, N., Blech, M., Pinnapireddy, S. R., Garidel, P., & Bakowsky, U. (2018). The application of STEP-technology(R) for particle and protein dispersion detection studies in biopharmaceutical research. *International Journal of Pharmaceutics, 543*(1–2), 257–268. https://doi.org/10.1016/j.ijpharm.2018.03.050

Hao, L. L., Sun, J. W., Pei, M. Q., Zhang, G. F., Li, C., Li, C. M., et al. (2022). Impact of non-covalent bound polyphenols on conformational, functional properties and in vitro digestibility of pea protein. *Food Chemistry, 383*, Article 132623. https://doi.org/10.1016/j.foodchem.2022.132623

Hati, S., Patel, M., & Yadav, D. (2018). Food bioprocessing by non-thermal plasma technology. *Current Opinion in Food Science, 19*, 85–91. https://doi.org/10.1016/j.cofs.2018.03.011

Huang, K., Shi, J. R., Li, M. Y., Sun, R. L., Guan, W. W., Cao, H. W., et al. (2022). Intervention of microwave irradiation on structure and quality characteristics of quinoa protein aggregates. *Food Hydrocolloids, 130*, Article 107677. https://doi.org/10.1016/j.foodhyd.2022.107677

Hu, Y. M., Guo, H. Z., Wang, H., Yang, Y. F., Tu, Z. C., & Huang, T. (2021). Insight into the mechanism of urea inhibit ovalbumin-glucose glycation by conventional spectrometry and liquid chromatography-high resolution mass spectrometry. *Food Chemistry, 342*, Article 128340. https://doi.org/10.1016/j.foodchem.2020.128340

Hu, Y. Y., Yang, S., Zhang, Y. C., Shi, L. F., Ren, Z. Y., Hao, G. X., et al. (2022). Effects of microfluidization cycles on physicochemical properties of soy protein isolate-soy oil emulsion films. *Food Hydrocolloids, 130*, Article 107684. https://doi.org/10.1016/j.foodhyd.2022.107684

Jermwongruttanachai, P., Pathaveerat, S., & Noypitak, S. (2021). Effect of temperature on thermal denaturation of skimmed coconut milk to produce a new product, coconut water. *Journal of Food Processing and Preservation, 45*(12), Article e16046. https://doi.org/10.1111/jfpp.16046

Ji, H., Tang, X. J., Li, L., Peng, S. L., Gao, C. J., & Chen, Y. (2020). Improved physicochemical properties of peanut protein isolate glycated by atmospheric pressure cold plasma (ACP) treatment. *Food Hydrocolloids, 109*, Article 106124. https://doi.org/10.1016/j.foodhyd.2020.106124

Kaavya, R., Pandiselvam, R., Gavahian, M., Tamanna, R., Jain, S., Dakshayani, R., et al. (2022). Cold plasma: A promising technology for improving the rheological characteristics of food. *Critical Reviews in Food Science and Nutrition*, 1–15. https://doi.org/10.1080/10408398.2022.2090494

Kotecka-Majchrzak, K., Sumara, A., Fornal, E., & Montowska, M. (2020). Oilseed proteins – properties and application as a food ingredient. *Trends in Food Science & Technology, 106*, 160–170. https://doi.org/10.1016/j.tifs.2020.10.004

Kunchitwaranont, A., Chiewchan, N., & Devahastin, S. (2019). Use and understanding of the role of spontaneously formed nanocellulosic fiber from lime (*Citrus aurantifolia* Swingle) residues to improve stability of sterilized coconut milk. *Journal of Food Science, 84*(12), 3674–3681. https://doi.org/10.1111/1750-3841.14937

Lei, X. Q., Qin, Z. W., Ye, B., Guo, F., Wu, Y., & Liu, L. (2022). Interaction between secondary lipid oxidation products and hemoglobin with multi-spectroscopic techniques and docking studies. *Food Chemistry, 394*, Article 133497. https://doi.org/10.1016/j.foodchem.2022.133497

Liao, X. Y., Cullen, P. J., Muhammad, A. I., Jiang, Z. M., Ye, X. Q., Liu, D. H., et al. (2020). Cold plasma-based hurdle interventions: New strategies for improving food safety. *Food Engineering Reviews, 12*, 321–332. https://doi.org/10.1007/s12393-020-09222-3

Li, R. J., Huang, L., Zhang, Z. W., Chen, J., & Tang, H. J. (2022). Integrated multispectroscopic analysis and molecular docking analyses of the structure-affinity relationship and mechanism of the interaction of flavonoids with zein. *Food Chemistry, 386*, Article 132839. https://doi.org/10.1016/j.foodchem.2022.132839

Li, J. G., Xiang, Q. S., Liu, X. S., Ding, T., Zhang, X. F., Zhai, Y., et al. (2017). Inactivation of soybean trypsin inhibitor by dielectric-barrier discharge (DBD) plasma. *Food Chemistry, 232*, 515–522. https://doi.org/10.1016/j.foodchem.2017.03.167

Li, M., Yang, R., Feng, X. C., Fan, X. J., Liu, Y. P., Xu, X. L., et al. (2022). Effects of low-frequency and high-intensity ultrasonic treatment combined with curdlan gels on the thermal gelling properties and structural properties of soy protein isolate. *Food Hydrocolloids, 127*, Article 107506. https://doi.org/10.1016/j.foodhyd.2022.107506

Lu, X., Su, H., Guo, J. J., Tu, J. J., Lei, Y., Zeng, S. X., et al. (2019). Rheological properties and structural features of coconut milk emulsions stabilized with maize kernels and starch. *Food Hydrocolloids, 96*, 385–395. https://doi.org/10.1016/j.foodhyd.2019.05.027

Misra, N. N., Yong, H. I., Phalak, R., & Jo, C. (2018). Atmospheric pressure cold plasma improves viscosifying and emulsion stabilizing properties of xanthan gum. *Food Hydrocolloids, 82*, 29–33. https://doi.org/10.1016/j.foodhyd.2018.03.031

Niu, H., Chen, X. W., Luo, T., Chen, H. M., & Fu, X. (2022). The interfacial behavior and long-term stability of emulsions stabilized by gum Arabic and sugar beet pectin. *Carbohydrate Polymers, 291*, Article 119623. https://doi.org/10.1016/j.carbpol.2022.119623

Nooshkam, M., Varidi, M., & Alkobeisi, F. (2022). Bioactive food foams stabilized by licorice extract/whey protein isolate/sodium alginate ternary complexes. *Food Hydrocolloids, 126*, Article 107488. https://doi.org/10.1016/j.foodhyd.2022.107488

Nyaisaba, B. M., Liu, X. X., Zhu, S. C., Fan, X. J., Sun, L. L., Hatab, S., et al. (2019). Effect of hydroxyl-radical on the biochemical properties and structure of myofibrillar protein from Alaska pollock (*Theragra chalcogramma*). *LWT - Food Science and Technology, 106*, 15–21. https://doi.org/10.1016/j.lwt.2019.02.045

Nyaisaba, B. M., Miao, W., Hatab, S., Siloam, A., Chen, M., & Deng, S. (2019). Effects of cold atmospheric plasma on squid proteases and gel properties of protein concentrate from squid (*Argentinus ilex*) mantle. *Food Chemistry, 291*, 68–76. https://doi.org/10.1016/j.foodchem.2019.04.012

Özaslan, Z. T., & İbanoğlu, Ş. (2022). Ozonation of corn starch in the presence of guar gum: Rheological, thermal and antioxidant properties. *Food Hydrocolloids, 124*, Article 107299. https://doi.org/10.1016/j.foodhyd.2021.107299

Paixao, L. B., Brandao, G. C., Araujo, R. G. O., & Korn, M. G. A. (2019). Assessment of cadmium and lead in commercial coconut water and industrialized coconut milk employing HR-CS GF AAS. *Food Chemistry, 284*, 259–263. https://doi.org/10.1016/j.foodchem.2018.12.116

Patil, U., & Benjakul, S. (2017). Characteristics of albumin and globulin from coconut meat and their role in emulsion stability without and with proteolysis. *Food Hydrocolloids, 69*, 220–228. https://doi.org/10.1016/j.foodhyd.2017.02.006

Rahmani-Manglano, N. E., Jones, N. C., Hoffmann, S. V., Guadix, E. M., Perez-Galvez, R., Guadix, A., et al. (2022). Structure of whey protein hydrolysate used as emulsifier in wet and dried oil delivery systems: Effect of pH and drying processing. *Food Chemistry, 390*, Article 133169. https://doi.org/10.1016/j.foodchem.2022.133169

Ramesh, S. V., Krishnan, V., Praveen, S., & Hebbar, K. B. (2021). Dietary prospects of coconut oil for the prevention and treatment of Alzheimer's disease (AD): A review of recent evidences. *Trends in Food Science & Technology, 112*, 201–211. https://doi.org/10.1016/j.tifs.2021.03.046

Ren, G. R., Shi, J. Y., Huang, S. J., Liu, C. Z., Ni, F. F., He, Y., et al. (2022). The fabrication of novel zein and resveratrol covalent conjugates: Enhanced thermal stability, emulsifying and antioxidant properties. *Food Chemistry, 374*, Article 131612. https://doi.org/10.1016/j.foodchem.2021.131612

Rodsamran, P., & Sothornvit, R. (2018). Physicochemical and functional properties of protein concentrate from by-product of coconut processing. *Food Chemistry, 241*, 364–371. https://doi.org/10.1016/j.foodchem.2017.08.116

Sadeghi, F., Koocheki, A., & Shahidi, F. (2021). Physical modification of *Lepidium perfoliatum* seed gum using cold atmospheric-pressure plasma treatment. *Food Hydrocolloids, 120*, Article 106902. https://10.1016/j.foodhyd.2021.106902.

Sharifian, A., Soltanizadeh, N., & Abbaszadeh, R. (2019). Effects of dielectric barrier discharge plasma on the physicochemical and functional properties of myofibrillar proteins. *Innovative Food Science & Emerging Technologies, 54*, 1–8. https://doi.org/10.1016/j.ifset.2019.03.006

Sharma, S., & Singh, R. K. (2022). Effect of atmospheric pressure cold plasma treatment time and composition of feed gas on properties of skim milk. *LWT - Food Science and Technology, 154*, Article 112747. https://doi.org/10.1016/j.lwt.2021.112747

Sun, F. S., Xie, X. X., Zhang, Y. F., Ma, M. Y., Wang, Y. Q., Duan, J. W., et al. (2021). Wheat gliadin in ethanol solutions treated using cold air plasma at atmospheric pressure. *Food Bioscience, 39*, Article 100808. https://doi.org/10.1016/j.fbio.2020.100808

Surojanametakul, V., Doi, H., Shibata, H., Mizumura, T., Takahashi, T., Varanyanond, W., et al. (2011). Reliable enzyme-linked immunosorbent assay for the determination of coconut milk proteins in processed foods. *Journal of Agricultural and Food Chemistry, 59*(6), 2131–2136. https://doi.org/10.1021/jf104067v

Tangsuphoom, N., & Coupland, J. N. (2009). Effect of surface-active stabilizers on the surface properties of coconut milk emulsions. *Food Hydrocolloids, 23*(7), 1801–1809. https://doi.org/10.1016/j.foodhyd.2008.12.002

Tiravibulsin, C., Lorjaroenphon, Y., Udompijitkul, P., & Kamonpatana, P. (2021). Sterilization of coconut milk in flexible packages via ohmic-assisted thermal sterilizer. *LWT - Food Science and Technology, 147*, Article 111552. https://doi.org/10.1016/j.lwt.2021.111552

Waghmare, R. (2021). Cold plasma technology for fruit based beverages: A review. *Trends in Food Science & Technology, 114*, 60–69. https://doi.org/10.1016/j.tifs.2021.05.018

Wang, Z. M., Zhou, H., Zhou, K., Tu, J. C., & Xu, B. C. (2022). An underlying softening mechanism in pale, soft and exudative - like rabbit meat: The role of reactive oxygen species - generating systems. *Food Research International, 151*, Article 110853. https://doi.org/10.1016/j.foodres.2021.110853

Wan, Z. L., Wang, L. Y., Wang, J. M., Zhou, Q., Yuan, Y., & Yang, X. Q. (2014). Synergistic interfacial properties of soy protein-stevioside mixtures: Relationship to emulsion stability. *Food Hydrocolloids, 39*, 127–135. https://doi.org/10.1016/j.foodhyd.2014.01.007

Xie, H. J., Ni, F. F., Gao, J., Liu, C. Z., Shi, J. Y., Ren, G. R., et al. (2022). Preparation of zein-lecithin-EGCG complex nanoparticles stabilized peppermint oil emulsions: Physicochemical properties, stability and intelligent sensory analysis. *Food Chemistry, 383*, Article 132453. https://doi.org/10.1016/j.foodchem.2022.132453

Xu, L., Hou, H., Farkas, B., Keener, K. M., Garner, A. L., & Tao, B. (2021). High voltage atmospheric cold plasma modification of bovine serum albumin. *LWT - Food Science and Technology, 149*, Article 111995. https://doi.org/10.1016/j.lwt.2021.111995

Yalegama, L. L., Nedra Karunaratne, D., Sivakanesan, R., & Jayasekara, C. (2013). Chemical and functional properties of fibre concentrates obtained from by-products of coconut kernel. *Food Chemistry, 141*(1), 124–130. https://doi.org/10.1016/j.foodchem.2013.02.118

Yang, J., Gu, Z., Cheng, L., Li, Z., Li, C., Ban, X., et al. (2021). Preparation and stability mechanisms of double emulsions stabilized by gelatinized native starch. *Carbohydrate Polymers, 262*, Article 117926. https://doi.org/10.1016/j.carbpol.2021.117926

Yang, S., Zhang, Q. L., Yang, H. Y., Shi, A. M., Dong, A. C., Wang, L., et al. (2022). Progress in infrared spectroscopy as an efficient tool for predicting protein secondary structure. *International Journal of Biological Macromolecules, 206*, 175–187. https://doi.org/10.1016/j.ijbiomac.2022.02.104

Yepez, X., Illera, A. E., Baykara, H., & Keener, K. (2022). Recent advances and potential applications of atmospheric pressure cold plasma technology for sustainable food processing. *Foods, 11*, 1833. https://doi.org/10.3390/foods11131833

Yuan, C., Liu, B. G., & Liu, H. (2015). Characterization of active ingredient-?-cyclodextrins with different substitution patterns via FTIR, GC-MS, and TG-DTA. *Carbohydrate Polymers, 118*, 36–40. https://doi.org/10.1016/j.carbpol.2014.10.070

Zhang, D. J., Zhang, Y. Y., Huang, Y. J., Chen, L., Bao, P. Q., Fang, H. M., et al. (2021). l-Arginine and l-Lysine alleviate myosin from oxidation: Their role in maintaining myosin's emulsifying properties. *Journal of Agricultural and Food Chemistry, 69*(10), 3189–3198. https://doi.org/10.1021/acs.jafc.0c06095

Zhang, Y. H., Zhou, F. B., Zhao, M. M., Lin, L. Z., Ning, Z. X., & Sun, B. G. (2018). Soy peptide nanoparticles by ultrasound-induced self-assembly of large peptide aggregates and their role on emulsion stability. *Food Hydrocolloids, 74*, 62–71. https://doi.org/10.1016/j.foodhyd.2017.07.021

Zhao, Q., Hong, X., Fan, L., Liu, Y., & Li, J. (2022). Solubility and emulsifying properties of perilla protein isolate: Improvement by phosphorylation in the presence of sodium tripolyphosphate and sodium trimetaphosphate. *Food Chemistry, 382*, Article 132252. https://doi.org/10.1016/j.foodchem.2022.132252

Zheng, Y. M., Li, Z. Y., Lu, Z. Y., Wu, F. H., Fu, G. M., Zheng, B. D., et al. (2022). Structural characteristics and emulsifying properties of lotus seed protein isolate-dextran glycoconjugates induced by a dynamic high pressure microfluidization Maillard reaction. *LWT - Food Science and Technology, 160*, Article 113309. https://doi.org/10.1016/j.lwt.2022.113309

Zhou, B. B., Tobin, J. T., Drusch, S., & Hogan, S. A. (2021). Interfacial properties of milk proteins: A review. *Advances in Colloid and Interface Science, 295*, Article 102347. https://doi.org/10.1016/j.cis.2020.102347

Zhou, R. W., Zhou, R. S., Zhuang, J. X., Zong, Z. C., Zhang, X. H., Liu, D. P., et al. (2016). Interaction of atmospheric-pressure air microplasmas with amino acids as fundamental processes in aqueous solution. *PLoS One, 11*(5), Article e0155584. https://doi.org/10.1371/journal.pone.0155584